

Tethering of the IgG1 Antibody to Amorphous Silica for Immunosensors development: A Molecular Dynamics Study

Didac Martí,^{1,2} Jon Ainsley,^{1,3} Oscar Ahumada,⁴ Carlos Alemán,^{1,2,} Juan Torras^{1,2,*}*

¹ Department of Chemical Engineering (EEBE). Universitat Politècnica de Catalunya, C/Eduard Maristany 10-14, Ed I2, 08019, Barcelona, Spain

² Barcelona Research Center for Multiscale Science and Engineering, Universitat Politècnica de Catalunya, C/Eduard Maristany 10-14, 08019, Barcelona, Spain

³ Cancer Therapeutics Unit, The Institute of Cancer Research, 15 Cotswold Road, Sutton, London SM2 5NG UK

⁴ Mecwins S.A., Ronda de Poniente 15, Tres Cantos, Madrid, 28760, Spain

***Corresponding Authors:** carlos.aleman@upc.edu and joan.torras@upc.edu

Abstract

A key factor for improving the sensitivity and performance of immunosensors based on mechanical-plasmonic methods is the orientation of the antibody proteins immobilized on the inorganic surface. Although experimental techniques fail to determine surface phenomena at the molecular level, modern simulations open the possibility of improving our understanding of protein-surface interactions. In this work, Replica Exchange Molecular Dynamics (REMD) simulations have been used to model the IgG1 protein tethered on amorphous silica surface considering a united-atom model and a relatively large system (2500 nm² surface). Additional Molecular Dynamics (MD) simulations have been conducted to derive an atomistic model for the amorphous silica surface using the cristobalite crystal structure as starting point and to examine the structure of the free IgG1 antibody in solution for comparison when immobilized. Analyses of the trajectories obtained for the tethered IgG1, which was sampled considering 32 different temperatures, have been used to define the geometry of the protein with respect to the inorganic surface. The tilt angle of the protein with respect to the surface plane increases with the temperature, the most populated value being 24°, and 66° and 87° at the lowest (250 K), room (298 K) and highest (380 K) temperature. This variation indicates that the importance of protein-surface interactions decreases with increasing temperature. The influence of the surface on the structure of the antibody is very significant in the constant region, which is directly involved in the tethering process, while it is relatively unimportant for the antigen-binding fragments, which are farthest from the surface. These results are expected to contribute to the development of improved mechanical-plasmonic sensor microarrays in the near future.

Introduction

Blood transfusion is one of the most common medical procedures used to save lives, globally around 85 million units of red blood cells are transfused in a given year.¹ This process consists of transferring blood or blood products into the circulatory system intravenously to treat a range of medical conditions that require the replacement of lost blood components. However, intravenous blood transfusions have drawbacks. The most important of such drawbacks is the window period of some viral diseases. Therefore, screening of donated blood is critical to prevent transfusion-transmissible infections, as for example Human Immunodeficiency Virus (HIV) and Hepatitis B or C. Currently, such screening processes are conducted using long and tedious immunological assays. For example, HIV testing is conducted with a p24 antibody-based test, which only provides reliable results 17 days after exposure to the virus by the donor. Although nucleic acid-based tests reduce the “*window phase*” to 10 days,² such tests are not feasible or affordable in underdeveloped regions. Therefore, a high sensitivity immunological assay would be highly valuable for infectious diseases.³

As HIV and Hepatitis viruses are not detectable in the first period after the initial infection (approximately the first three weeks up to six months⁴) due to the very low concentration of detectable agents in blood, blood transfusion has to meet very high standards of product safety. Accordingly, novel detection platforms using new sensing technologies are necessary to improve the safety. A few years ago, a technology based on silicon cantilevers was proposed for the ultra-sensitive detection of protein cancer biomarkers in blood.⁵ The sensor is based on a double signature, combining the functionalization of the cantilever with an antibody and a second antibody free in the solution that is bound to a gold nanoparticle (GNP) with plasmonic properties. The second antibody recognizes a free region of the analyzed biomarker. The silicon

cantilever acts as a mechanical resonator for weighting the mass of the captured nanoparticles and as optical cavity due to the two reflective opposite surfaces, which boosts the plasmonic signal from GNPs. The combination of mechanical and optical response exhibited a great potential to surpass the current industry standard methods in terms of sensitivity to infectious agents of blood-borne pathogens.⁵⁻⁷

Extension of this technology to other biomarkers different from the carcinogenic ones, as for example the HIV or hepatitis viruses, is a technological challenge. The first one is the substitution anti-cancer antibodies used in previous work⁵ by an anti-virus antibody. In this work we have selected an isotype of immunoglobulin G (IgG) that can bind specifically to a HIV antigen as a detection target.⁸ The IgG is the immunoglobulin found with the highest concentration in blood (800 to 1600 mg/100 mL), being one of the most abundant proteins in human serum (10-20% of plasma protein). Moreover, it presents high specificity for virus antigens, playing a decisive role within the passive immune system and protecting against bacterial and viral infections, including HIV.^{8,9}

Figure 1a shows the mechanism used by the combined mechanical-plasmonic technology, in which the antibodies used for cancer biomarkers detection are replaced by IgG.⁵ The detection mechanism is based on the formation of a “*sandwich*” between the sensor surface (*i.e.* amorphous silica) and the GNP. Both elements are functionalized with IgG and can bind specifically to an antigen as a detection target. The orientation of the sensing antibody with respect to the surface should be the optimal after its adsorption. Such optimum orientation is a crucial requisite for maintaining the IgG biological activity and, therefore, for reaching the most sensitive antigen detection limit.¹⁰ Accordingly, the definition of the optimum orientation is essential for the future development of mechanical-plasmonic transduction bioassays, enabling to

detect ultra-low amounts of virus biomarkers by eliminating undesired denaturation and deformation effects as well as the inaccessibility of the antigen binding site.

IgG is a large globular protein with a molecular weight of ~ 150000 Daltons, made of four peptide chains: two heavy (H) chains with 446 amino acid residues and two light (L) chains with 214 amino acid residues each (Figure 1b). Several disulfide bonds crosslink these chains into a flexible Y-shaped structure with dimensions of approximately $14.5 \text{ nm} \times 8.5 \text{ nm} \times 4.0 \text{ nm}$.¹¹ The antigen-binding fragments (Fab), which are variable regions situated in the upper arms side of Y-shape, contain the antigen binding site (ABS) at their tips, whereas the vertical part of the “Y” named Fc, represents the constant region.

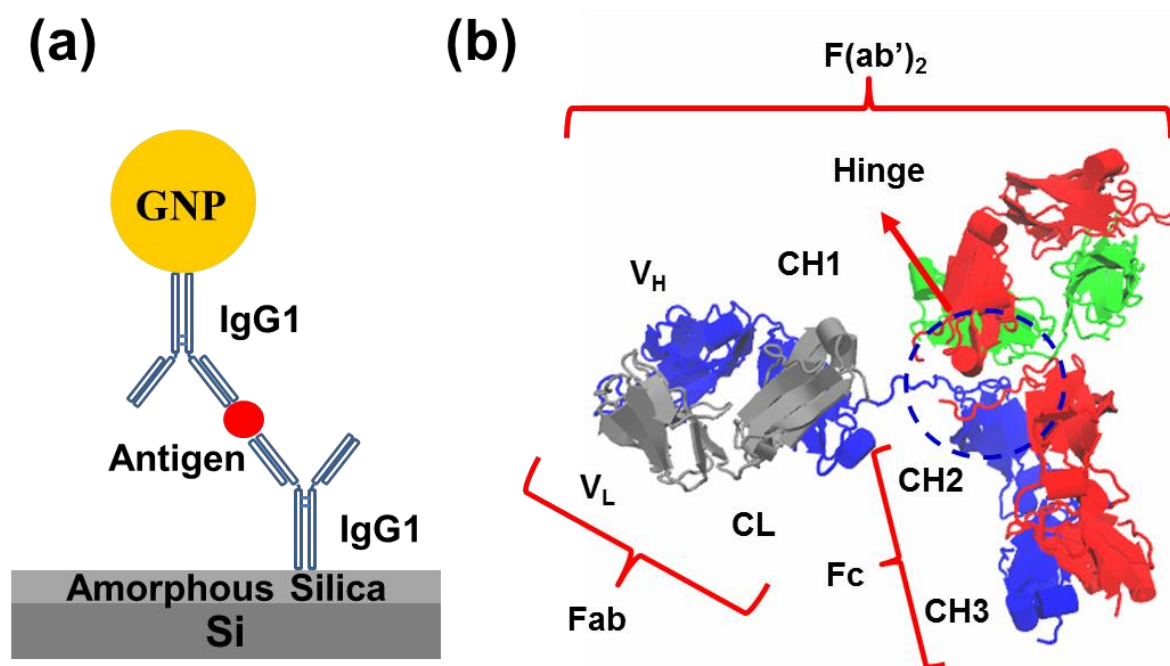


Figure 1. (a) Sandwich complex formed to catch antigens between the antibodies immobilized at the amorphous silica surface and the GNP. (b) Sketch of the structure of the human IgG antibody, indicating the position of the variable and fixed regions (Fab and Fc, respectively). The sub-chains composition is also detailed for the heavy (V_H , CH_1 , CH_2 , and CH_3) and light (V_L and CL) chains.

Considering its complex structure, IgG could easily be denatured by shape deformation when adsorbed on the silica cantilever, as has found for other soft macromolecules with complicated shapes.¹² In addition, the specific location of the antigen binding sites (Figure 1b) makes the orientation of immobilized IgG on the surface an important factor to its final functional activity. Indeed, the influence of environmental conditions (*e.g.* ionic strength, pH, and surface charge) on the IgG orientation and, thus, its activity when printed by microcontact on oxygen-plasma cleaned glass substrate was early proved.¹³

Computational techniques based on molecular simulations are useful tools able to provide relevant information on complex protein-surface systems at the microscopic level. However, chemisorption simulation studies on IgG systems are challenging due the large size of such antibody. In fact, the modeling of the chemisorbed IgG protein has been studied using different degrees of approximation in the few previous works reported in the literature.¹⁴⁻¹⁷ In an early study, Zhou *et al.*¹⁴ explored the conformational orientations of IgG1 and IgG2a applying Monte Carlo (MC) simulations to a coarse-grained model, in which each amino acid was reduced to a single sphere centered at the α -carbon position. Later on, the same group used parallel tempering MC and all-atom Molecular Dynamics (MD) simulations to model a fragment of the IgG protein in a short amorphous silica surface,¹⁵ while Cooper *et al.*¹⁶ employed a Poisson-Boltzmann model to examine the effect of the surface charge on the orientation of the protein. More recently, Grawe and Knotts¹⁷ proposed a coarse-grained model with one bead per amino acid residue to study the IgG stability on surfaces using Replica Exchange Molecular Dynamics (REMD). On the other hand, MD has been proved a reliable simulation technique as demonstrated for different enzymes by comparing the predicted orientation with the

experimental ones, which were obtained using sum frequency generation (SFG) vibrational spectroscopy and attenuated total reflection Fourier transform infrared (ATR-FTIR) spectroscopy.^{18,19}

The main objective in this work is to examine the chemisorption mode of human IgG1, which is most abundant subclass of immunoglobulin G,⁸ on a silica cantilever using a united atom model that only neglects the explicit description of hydrogen atoms attached to carbon. More specifically, the structure and the orientation of the protein on the surface, which will determine the bioactivity, as well as its specificity have analyzed in detail. For this purpose, REMD simulations on a IgG1-silica surface model have been conducted to obtain a good potential sampling of the surface and antibody interactions, allowing us to obtain a wide spectrum of possible conformations. Overall, results derived from this study are useful to build better mechanical-plasmonic sensor arrays.

Methods

Silica surface model

The main sensor surface is made of a silicon crystal with a 10 nm thin layer of amorphous silica on the top side of the surface, on which the antibody is deposited, in contact with the final solution (Figure 1a). Consequently, a slab of amorphous silica was built to simulate the outermost sensor surface. This was performed by applying the procedure reported by Huff *et al.*²⁰ to convert α -cristobalite into amorphous silica. More specifically, a α -cristobalite slab of $50 \times 50 \times 20 \text{ \AA}^3$ was constructed and, subsequently, subjected to a rigorous annealing process by applying several heating and quick cooling processes. The annealing process was conducted

using a MD approach as implemented in the DLPOLY 4 program²¹ and applying the Tersoff potential for bulk silica.²² Details are provided in the Electronic Supporting Information.

IgG1 protein model

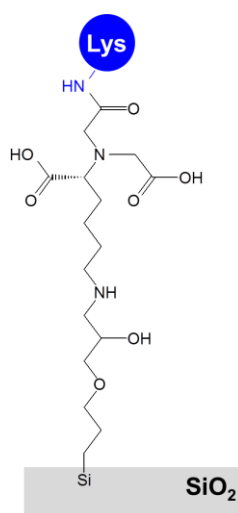
The initial crystal structure of IgG1, which was at 2.7 Å resolution, was extracted from the Protein Data Bank (ID: 1HZH). More specifically, we used the human antibody IgG1 b12, which recognizes a conserved epitope of the CD4-binding protein gp120 of the human immunodeficiency virus-1 (HIV-1), and is one of the antibodies capable of potent neutralization of primary HIV-1.²³

The protein crystal structure was solvated in a water box of $156 \times 147 \times 205 \text{ \AA}^3$ containing 147712 water molecules. The system was equilibrated to constant density and relaxed during 180 ns using a NVT ensemble at 298 K of classical MD in AMBER 18 software.²⁴ Water molecules were described using the TIP3P model,²⁵ whereas protein molecular interactions were described by the ff14SB Amber force-field.²⁶ The relaxed IgG1 system in explicit water was used to construct the model of chemisorbed IgG1 on the silica surface.

Immobilized IgG1 on amorphous silica surface

Various techniques have been reported to immobilize antibodies on different surfaces for immunoassays.²⁷ In this work, the IgG1 protein has been considered attached to the amorphous silica surface by means of the protocol described by Puiggali-Jou *et al.*,²⁸ which has been successfully used to immobilize different kind of proteins on nanomechanical silica cantilevers.²⁹ More specifically, the functionalized surface was activated by means of a mixture of 1-[(3-dimethylamino)propyl]-3-ethylcarbodiimide methiodide (EDC) and N-hydroxysuccinimide

(NHS). Finally, the protein was immobilized by incubating the activated surface in the corresponding protein solution. This technique specifically binds the Fc portion of IgG1 to the surface, thus allowing large oriented systems.³⁰ Scheme 1 shows the surface with the final linker molecule structure used to attach IgG1 to the surface, the terminal amino group of Lys side chain being where the linker binds. Consequently, a new modified amino acid, which consists on Lys with the linker molecule bonded to its side chain, was built for the simulations. The modified amino acid was included within the sequence of the Fc region of the IgG1 antibody.



Scheme 1. Detail of the linker molecule used to tether the IgG1 antibody to the surface.

The modified protein was linked to a silicon atom of the silica surface. The linker-surface bond distance was estimated by quantum mechanics (QM) using density functional theory (DFT) calculations at B3LYP/6-31G level, as is implemented in the Gaussian09 software.³¹ DFT calculations were performed in a small model system consisting of the linker molecule that bound to a small tetrahedral silica unit (-SiO₃) at one end and to the amino group of Lys side chain at the other end. This model system was also used to obtain the point charges of the linker-Lys residue, which are necessary for carrying out the classical MD simulations.

The modified linker-Lys residue and the rest of the IgG1 protein were described under the united-atom ff03ua AMBER force-field.³² Although the amorphous silica substrate was kept frozen along all classical simulations, both the coulombic and van der Waals interactions induced by the silica were allowed to influence the rest of the system. The point charges and van der Waals parameters used to describe the amorphous silica slab were taken from the literature.³³ Both the size of the simulation box and the huge number of explicit particles contained in the IgG1-surface complex (*ca.* ~379,000 atoms) made impossible the inclusion of explicit water molecules. Accordingly, the aqueous environment was represented using the generalized Born implicit solvent (GBIS).³⁴ The GBIS implicit model, which approaches the polar solvent as a dielectric continuum, is extensively used for modeling large systems like the one studied in this work.³⁵⁻³⁸ Figure 2 shows the IgG1 antibody immobilized on amorphous silica, which is the system to be simulated.

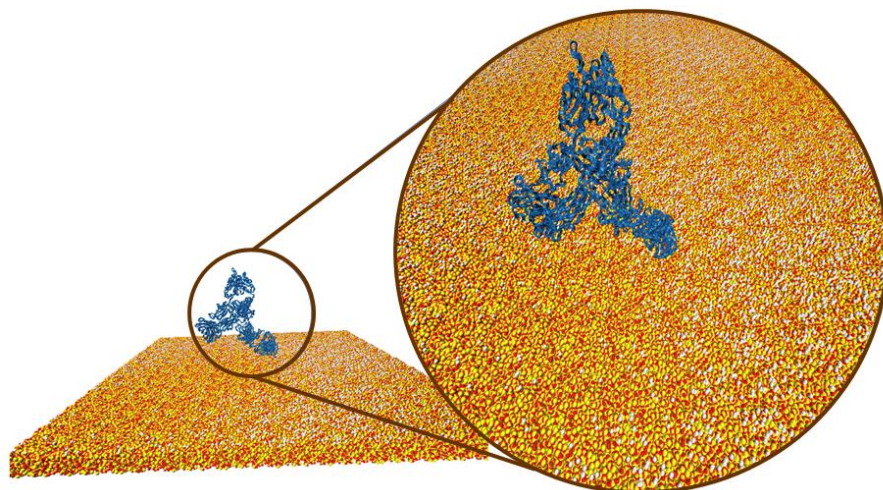


Figure 2. Human IgG1 antibody immobilized on amorphous silica surface ($50 \times 50 \times 2 \text{ nm}^3$).

Replica exchange molecular dynamics protocol

The studied system was simulated using the REMD methodology^{38,39} as implemented in the NAMD 2.13 software package.⁴⁰ REMD is a technique used to enhance sampling relative to standard MD simulations by allowing systems of similar potential energies to sample conformations at different temperatures. By applying this procedure, energy barriers on the potential energy surface can be overcome, allowing exploration of different regions of the conformational space.⁴¹ The system, number of replicas, range of temperature space and the distribution of temperatures determine the average exchange probability between each replica. A total of 32 replicas were exponentially distributed from temperatures of 250.0 K up to 380.0 K.

Simulations were run in the Barcelona Supercomputer Center's (BSC's) Minotauro GPU cluster using a total amount of 32 GPUs (one per temperature). 15 ns of REMD trajectories per temperature were obtained, using an attempt to exchange every 1.0 ps between all neighboring replicas with final average acceptance rates of 25%. All trajectories resulted in a cumulative simulation time of 400 ns of REMD. Simulations were conducted using a Langevin thermostat with a friction coefficient of 5.0 ps^{-1} , an integration time step of 2 fs, and a cutoff of 16 Å. Each replica was previously equilibrated by a set of short runs at constant temperature of 0.5 ns to ensure that the target temperature was reached. REMD data were collected from the last 11.0 ns of each simulation at the lowest targeted temperature of 250 K and at the common targeted temperature of 298 K to perform the data analyses.

Results and Discussion

Silica surface structure

The discussion the modeled slab of amorphous SiO₂ (Figure S1) is provided in the Electronic Supporting Information. The final density of the SiO₂ glass was 2.22 g/cm^3 , which perfectly

matches the experimental value of 2.20 g/cm³.⁴² Similarly, the structure of the proposed model, as derived from analyses of the calculated radial distribution functions (RDFs), is very close to experimental one^{42,43} (Table S1) and similar to those previously reported using other force fields.^{44,45} The SiO₂ glass obtained was next used to model a large slab of amorphous silica by replicating along the *xy* plane. The hydroxylation process (see Supporting Information) leads to a density of hydrogen atoms per nm² close to the one experimentally determined on freshly fractured SiO₂ surfaces (2.6 hydrogen atoms per nm²).⁴⁶

Study of the antibody in aqueous solution with explicit solvent molecules

The crystallographic structure of IgG1 was equilibrated and relaxed in aqueous solution using an explicit water model (*i.e.* 147712 TIP3P water molecules). After a production trajectory of 180 ns, the conformational changes induced by explicit solvation were carefully examined. Figure 3a shows the temporal evolution of the root mean square displacement (RMSD) of the IgG1 backbone along the whole MD relaxation. After 30 ns, the IgG1 reaches a steady state with some oscillations between two different conformational states, which correspond to the maxima and minima in the steady zone of the RMSD profile. This reflects the existence of some flexible protein parts within the main IgG1 structure. More specifically, structural differences are mainly located on the hinge and the loop of the Fc region that present less structural compactness in the conformations with the highest RMSD value. Figure 3b displays the root mean square fluctuation (RMSF) of the C^α atom of all protein residues, measuring the displacement of C^α atoms with respect to their crystallographic positions. The RMSF shows four groups of C^α atoms that exhibit higher displacement than the others have, which have been identified as the VH, CH1, VL and CL regions from the arms of the IgG1 Y-shaped structure (see Figure 1b).

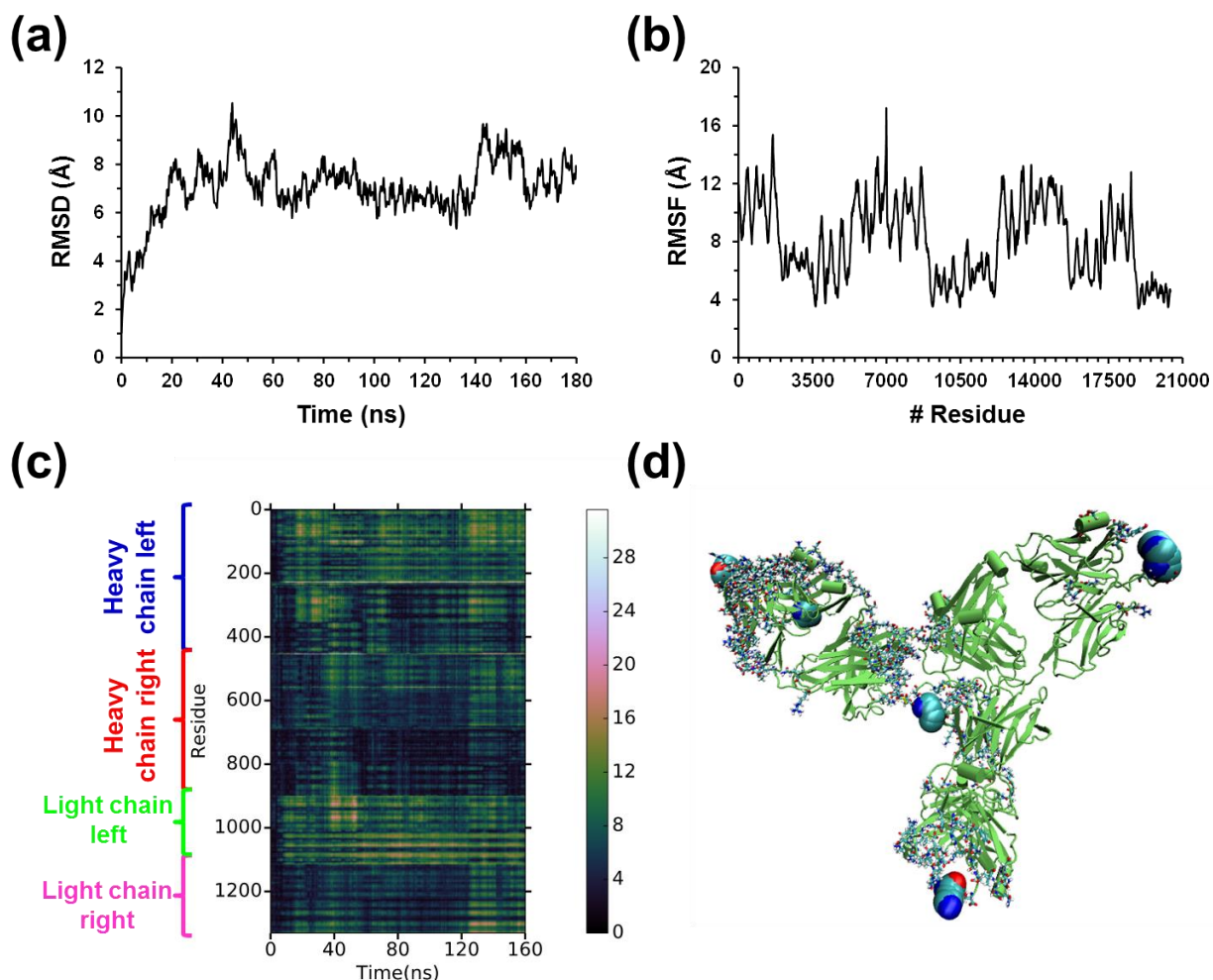


Figure 3. (a) Temporal evolution of the RMSD and (b) RMSF plot of the C^α for IgG1 during the MD in aqueous solution. (c) RMSD per residue heat-map (scale 0–30, from low/black to high/white) for IgG1 in explicit water. (d) IgG1 protein picture showing the hottest residues (large spheres representation), the warm residues (licorice representation), and the coldest residues (green cartoon backbone representation).

The RMSD per residue heat-map of the IgG1 protein in explicit water for the whole MD trajectory is shown in Figure 3c. Five residues of the heavy chains present the longest displacements. More specifically, those residues, which are depicted in Figure 3d, are located close to the hinge (Lys232) and at the three ending residues of each extreme of the Y-shape structure (*i.e.* Trp104, Asp105 and Trp561 of the Fab region, and Lys457 of the Fc region). Also,

there is a large group of residues with intermediate displacements, which are mainly located at the less flexible V_L , V_H and CH2 chains (Figure 3d). Indeed, a close inspection to the initial and final conformations of the trajectory in solution reveals that the IgG1 protein adopts a more compact conformation in relation to the crystallographic structure used as starting point. This is confirmed by the calculated radius of gyration that decreases from 51.1 Å at the beginning of the production run to 49.6 Å at the end of the simulation.

Immobilized Antibody

An exhaustive conformational study on the IgG1 antibody chemisorbed on an amorphous silica surface was conducted by means of REMD approach. For this purpose, 32 replicas were carried out in NVT ensemble for 15 ns with an exponential temperature distribution between 250.0 and 380.0 K. Exchanges between neighboring replicas were attempted every 1.0 ps, the final average acceptance rates being of 25%. Figure 4 shows representative snapshots at selected temperatures, which illustrates the large influence of the temperature on the immobilization of the antibody. Since the most energetic conformations were populating the trajectories at the higher temperatures, conformational analyses of immobilized IgG1 structures were mainly focused trajectories at two temperatures of interest. These are the trajectory at lowest temperature (250 K), which is populated with the most stable conformations, and the trajectory at 298 K that can be directly compared with the simulation of free IgG1 in aqueous solution, which was conducted using explicit water molecules. However, in order to evaluate the influence of the temperature on the relative disposition of immobilized IgG1, some analyses were also conducted at the highest temperature (380 K). Considering the temporal evolution of the RMSD for the

trajectories at different temperatures (Figure S2), the conformational analyses of immobilized IgG1 were performed using the last 11 ns of each trajectory.

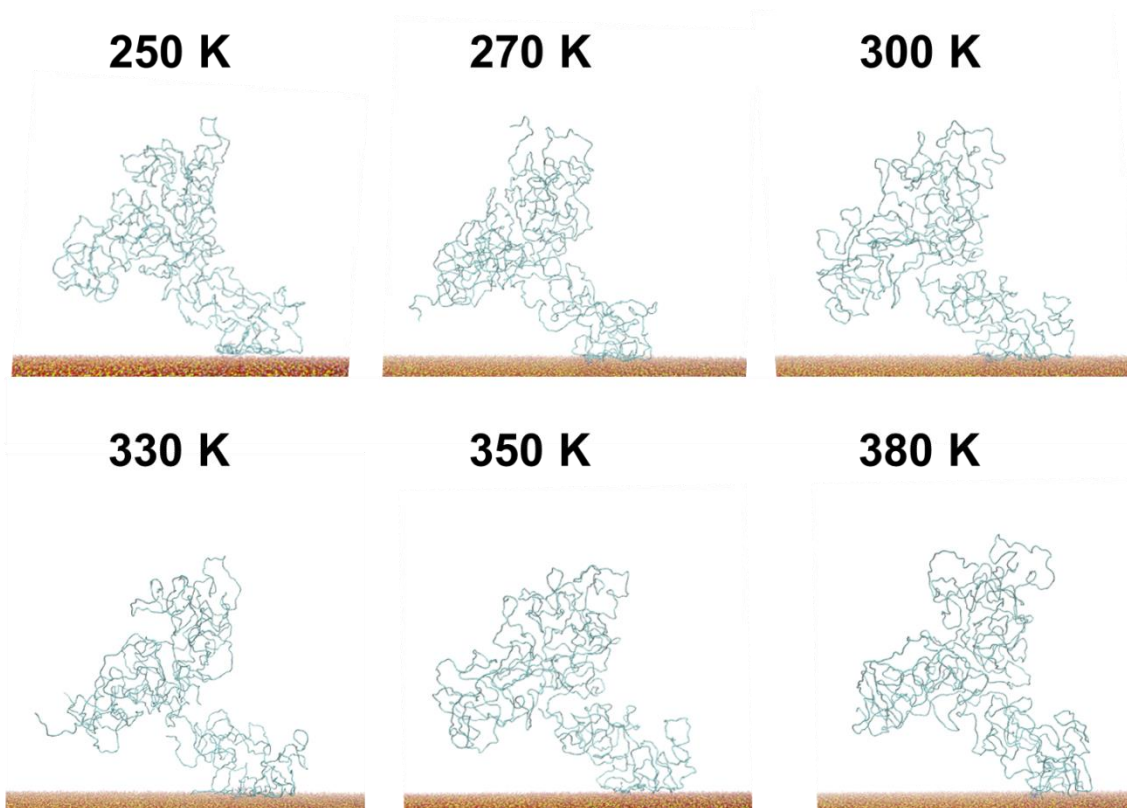
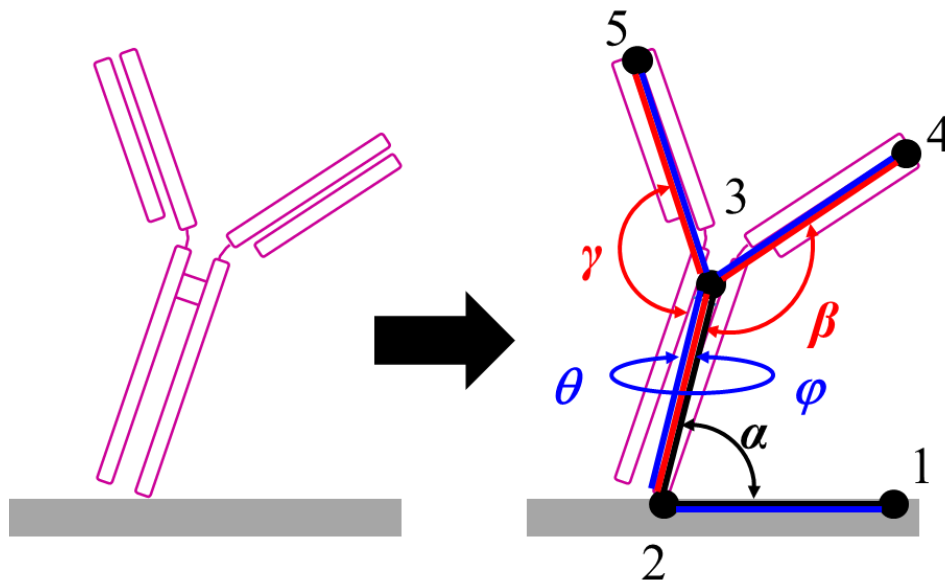


Figure 4. Representative snapshots recorded at selected temperatures.

The radius of gyration (R_g) of the free and immobilized IgG1 protein are compared in Table S2. The variation in the R_g values indicates that the presence of the amorphous silica surfaces affects not only the compactness but also the shape of the IgG1 structure. More specifically, R_g increases from 49.8 Å for the free protein in aqueous solution to 56.3-56.4 Å for the tethered protein, evidencing the silica surface produces a less compact but more elongated structure. In addition, such R_g increment is not distributed homogeneously in the three spatial directions. Inspection to the three components of R_g reveals that the elongation is mainly located along the

xz plane, where R_g^x and R_g^z present the largest increments. This results in a deformation of the shape along the x - and z -axes with respect to the structure of the free protein.

Analysis of the influence of the amorphous silica surface on the conformation of IgG1 was conducted along all the REMD simulation. Five different angles were evaluated for each temperature's trajectory. Scheme 2 shows the meaning of such angles, where the numbered black spots are used to help for describing each geometric parameter. More specifically, α corresponds to the tilting angle of the protein with respect to the surface (described by 1-2-3 linkage), β is the angle between the surface linkage atom of the IgG1 and one of the Fab branches (2-3-4 linkage), and φ is the dihedral angle involving the rotation of this branch with respect to the surface (1-2-3-4 linkage). Similarly, γ and θ angles describe the Fab' antibody branch.



Scheme 2. Structural angles between the IgG1 protein and the amorphous silica surface. α is the angle between the surface and the Fc branch (1-2-3); β is the angle between Fc and one of the Fab (2-3-4); γ is the angle between Fc and the other antibody branch structure (2-3-5); φ and θ are the dihedral angles between surface, Fc and each one of the Fab branches (1-2-3-4 and 1-2-3-5, respectively).

Figure 5 shows the histograms obtained at 250, 298 and 380 K for α angle between the antibody with the amorphous silica surface and the θ and φ dihedral angles of the Fab and Fab' branches, respectively, with an imaginary xz plane perpendicular to the sensor surface. Results derived from the trajectory at 250 K, which exhibits the accumulation of the most energetically favored conformations, reflect that the most populated α angle presents a very low value ($\alpha = 24^\circ$). This indicates that the Fc region is very close to the silica surface favoring protein-surface interactions and stabilizing the system. When the temperature increases to 298 K, the most populated α angle shifts to 66° (Figure 5a), evidencing a lower influence of the interactions between the IgG1 protein and the anchoring surface. However, the local maxima are less defined in the latter case than at 250 K, which has been attributed to the increasing kinetic energy. This tendency is confirmed by the broad histogram recorded at 380 K, which exhibits $\alpha = 87^\circ$ as the most populated value (*i.e.* the protein is roughly perpendicular to the amorphous silica surface). This result indicates that the orientation of the IgG1 with respect to the anchoring silica surface can be tuned with the temperature, which exerts an important effect on the protein-surface interactions.

The histograms calculated for the angles between the Fc and the two Fab regions, β and γ , are shown in Figure 5b-c. The most populated values detected at 250 °C, which appear at 69° - 72° and 54° , respectively, shift to higher values (*e.g.* 102° and 75° at 380 K, respectively) when the temperature increases. This indicates that the contribution of protein-protein interactions grows with respect to protein-surface interactions with increasing temperature, which is fully consistent with the behavior found for the α angle. Despite of this, the angle β and γ experience a marked decrease when the protein is immobilized on the silica surface with respect to the values obtained in solution. This reflects the silica-induced deformation of the Fab regions, even though this

phenomenon can be in part mitigated by increasing the temperature. In fact, hydration without the surface presence promotes an equidistant distribution between the two Fab and the Fc regions with average angles close to those of an equilateral triangle. More specifically, $\beta = 118^\circ \pm 7^\circ$ and $\gamma = 131^\circ \pm 6^\circ$ values were measured for the free IgG1 protein in solution.

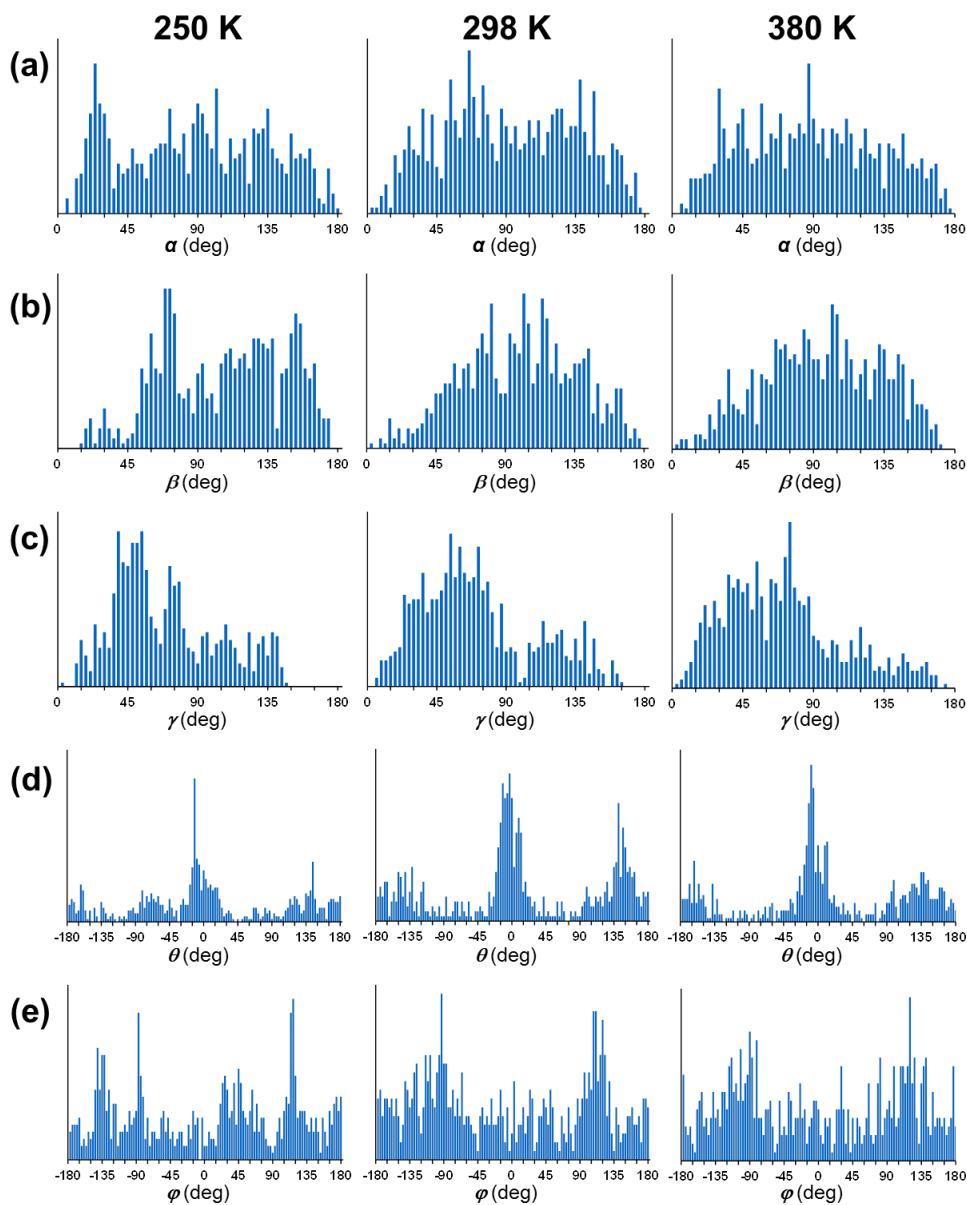


Figure 5. Histograms of the (a) α , (b) β and (c) γ angles, and the (d) θ and (e) ϕ dihedral angles (see Scheme 2) for the IgG1 tethered on the amorphous silica surface. Histograms have been calculated for trajectories at 250 K (left), 298 K (middle) and 380 K (right).

The θ dihedral angle (Figure 5d) shows several maxima at similar positions for 250, 298 and 380 K trajectories, even though the distributions around the most populated angles (*i.e.* $\theta = -12^\circ$, -3° and -9° at 250, 298 and 380 K, respectively) are better defined at the former temperature than at the latter ones, as occurred for α , β and γ . Table S3 lists the most populated maxima (sorted by population in descending order) for the structural parameters described in Scheme 2 as derived from the trajectories at 250 and 298 and 380 K. In general, the number of local maxima decreases with increasing temperature, the values for the most populated being similar in all cases with exception of α and φ . However, the latter two parameters exhibit important differences at the compared temperatures. The main differences involving the α angle have already been discussed above, while the φ dihedral angle exhibits a dichotomous angle population distributed between values of $\varphi = -93^\circ$ and 117° (Figure 5e). This heterogeneous distribution becomes less pronounced with increasing temperature, even though it is still observed at 380 K. This behavior is confirmed by the average among all the populated angles in the whole range of REMD temperatures (Table S3). Thus, the average obtained by considering the runs at all temperatures are quite similar for all the geometric parameters with exception of the φ dihedral angle, which presents two different populations systematically revisited along all temperatures (*i.e.* -94° and 116°).

LaGraff *et al.*¹³ studied the IgG1 deposition on a glass surface. A monolayer with a thickness of 5 nm was observed on the surface, which was attributed to a flat lay arrangement of IgG1 protein. When the second IgG1 layer was deposited, the thickness increased by 15 nm, suggesting that the protein adopted a more vertical deposition in the second layer than in the first one. This is fully consistent with the computational results displayed in the present work, which

shows that the most stable structures at 250 and 298 K temperature exhibit a small α tilt angle ($\alpha= 24^\circ$ and 66° , respectively). Thus, structures with greater surface interaction are favored, which explain the laid-flat or end-on deposition (*i.e.* Fc near the surface and F(ab')₂ away from the surface) reported experimentally.^{13,47} However, the histograms displayed in Figure 5 indicate that this effect can be corrected by raising the temperature.

Grawe *et al.*¹⁷ used computational simulations within the framework of the coarse-graining approximation to study the stability of an IgG antibody on hydrophobic and hydrophilic surfaces. The antibody showed greater stability on hydrophilic surfaces than on hydrophobic surfaces, even though a significant degree of denaturation was obtained in both cases. Therefore, the study of the influence of the amorphous silica surface on the structural stability of the IgG1 antibody deserves consideration. In this work, the structural stability of the tethered protein has been determined by measuring the distance of the different IgG1 regions to the inorganic surface. More specifically, the perpendicular distances between the center of mass of the Fc, Fab and Fab' regions and the amorphous silica surface (hereafter named d_{z-Fc} , d_{z-Fab} and $d_{z-Fab'}$, respectively) were computed and averaged considering the last part of the trajectory at each temperature. The distances measured for the starting structure geometry of REMD simulations, which was obtained after the IgG1 simulation in aqueous solution and, therefore, was not affected by the inorganic surface, were used as the reference of the non-denatured state: $d_{z-Fc}= 37.0 \text{ \AA}$, $d_{z-Fab}= 111.9 \text{ \AA}$, and $d_{z-Fab'}= 71.5 \text{ \AA}$. These parameters were expected to be very sensitive to conformational changes and, therefore, able to detect structural variations, as the denaturation found by coarse-grained simulations.¹⁷

Figure 6a represents the evolution of the d_{z-Fc} distance against the simulated temperatures. The distance of center of mass of the Fc region to the surface varies between 26.1 \AA at 318.8 K and

27.7 Å at 380 K, even though it remains between 26.1 and 26.8 Å in a wide temperature range (*i.e.* from 250 K to 345.7 K). The average of the d_{z-Fc} over the entire temperature range, 26.6 ± 0.4 Å, is 28% lower than the value of the starting structure. This reduction indicates that the chemical adsorption of the IgG1 protein causes denaturation in the Fc region, which is the closest to the amorphous silica surface. On the other hand, the maximum variation of d_{z-Fab} and $d_{z-Fab'}$ with the temperature is of ~ 1 Å only, indicating that the Fab and Fab' are not influenced by the surface (Figure 6b-c). Indeed, the average values for the whole temperature range are $d_{z-Fab} = 112.2 \pm 0.2$ Å and $d_{z-Fab'} = 69.8 \pm 0.2$ Å, which represent a deviation with respect to the initial structure of only 0.3% and 2.4%, respectively.

Other geometric parameter that supports the effect of the surface on the Fc region tethered IgG1 protein are the interchain distance. This parameter, which was calculated as the distance between the centers of mass of the two heavy chains constituting the Fc region (d_{Fc}) is represented in Figure 6d. The interchain distances measured in the structure used as starting geometry for the simulations of the immobilized protein is $d_{Fc} = 25.9$ Å, while the total average is $d_{Fc} = 37.9 \pm 0.5$ Å. This important difference ($\Delta d_{Fc} = 12.0$ Å) reflects the large impact of the amorphous silica surface on the Fc region, which results largely destabilized.

This result, which is consistent with the low value of the α angle, is graphically illustrated in Figure 6e. Comparison of the structures recorded for the protein at the beginning (Figure 6e, left) and at the end (Figure 6e right) of the trajectory run at 298 K evidences that the structural destabilization is much greater in the Fc region than in the Fab and Fab' ones. However, it should be taken into account that the simulations reported in this work for the immobilized protein were conducted using an implicit water model, which probably contributes to overestimate the strength of protein-surface interactions. Unfortunately, the utilization of an

explicit solvent model was computationally prohibitive since the large size of the model used for the silica surface required a huge amount of water molecules. Therefore, the results obtained in this work for the Fc region should be considered as the maximum threshold in terms of structural destabilization.

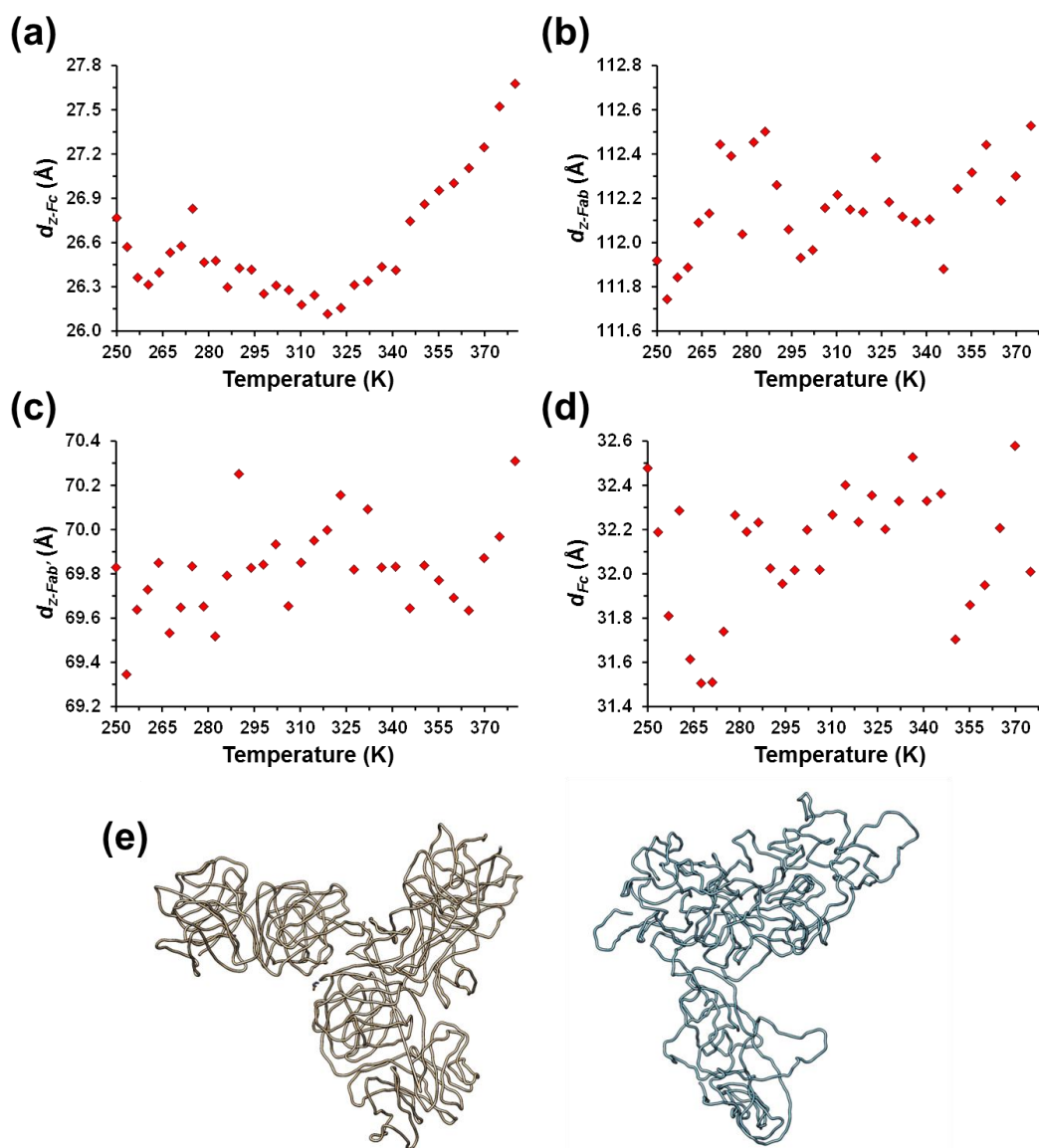


Figure 6. Geometric parameters used to examine the influence of the silica surface on the structural stability of the immobilized IgG1 protein: (a) perpendicular distance between the center of mass of the Fc region and the surface (d_{z-Fc}); (b) perpendicular distance between the center of mass of the Fab region and the surface (d_{z-Fab}); (c) perpendicular distance between the

center of mass of the Fab' region and the surface ($d_{z-Fab'}$); and (d) distance between the centers of mass of the two heavy chains constituting the Fc region (d_{Fc}). (e) Representative snapshots showing the backbone of the protein at the beginning (left) and at the end (right) of the trajectory recorded at 298 K. The silica surface is not displayed for clarity.

Conclusions

An atomistic model that only neglects the hydrogen atoms attached to carbon has been used to model the IgG1 immunoglobulin chemisorbed on a silica cantilever. For this purpose, an amorphous silica glass model has been obtained applying a simulated annealing process. The model's fidelity has been demonstrated by comparing the calculated structural properties with previous experimental values. The IgG1 X-ray crystal structure was equilibrated with explicit water before being immobilized on the silica glass surface. A heat-map of the solvated protein indicates that the lowest part of the Y-shape structure presents the greatest displacement, the four residues with the largest displacement corresponding to the three ends of the Y-shape and the hinge. Then, the IgG1 protein was anchored to the amorphous silica surface by bonding a Lys residue of the Fc region to a flexible linker derived from EDC chemistry. REMD trajectories were run over 32 different temperatures and, subsequently, analyzed. The structures obtained at the lower temperatures exhibited more interactions with the surface, as reflected the low values of the angle α as well as other geometric parameter designed to measure the tilt between the surface and the Fc region of the IgG1 protein. Thus, the most populated angle α at room temperature presented a value of 66° , while the value averaged over the all the temperature range increased to $82^\circ \pm 26^\circ$.

The orientation of tethered proteins is important for immunoassays since highly oriented antibodies could result in an improvement in the sensitivity of biosensors.⁴⁸ This study increases

our understanding of how the IgG1 protein is affected by amorphous silica cantilevers. Further work will be focused on two different aspects of mechanical-plasmonic transducers for HIV. First, the interaction of immobilized IgG1 with a second antibody will be modeled to progress in the development of mechanical-plasmonic sensors for HIV. It is expected that such IgG1-antibody interactions alleviate the effect of the IgG1-surface interactions. Second, additional simulations will be conducted on a reduced model for the immobilized IgG1 using explicit solvent molecules. These simulations will provide relevant information about how implicit solvation models exaggerate the destabilization of the tethered protein by overestimating of the protein-surface interactions.

Acknowledgements

This work was supported by MINECO-FEDER (RTC-2017-6311-1) and the Agència de Gestió d'Ajuts Universitaris i de Recerca (2017SGR359). The authors would like to acknowledge RES to give access to Mare Nostrum at Barcelona Supercomputer Centre. Support for the research of C.A. was received through the prize “ICREA Academia” for excellence in research funded by the Generalitat de Catalunya.

Supporting Information

Density and geometric parameters of amorphous silica; radius of gyration for the free and immobilized IgG1 protein; geometric parameters used to define the orientation of immobilized IgG1; and temporal evolution of the RMSD of IgG1 immobilized on amorphous silica.

References

1. Carson, J. L.; Grossman, B. J.; Kleinman, S.; Tinmouth, A. T.; Marques, M. B.; Fung, M. K.; Holcomb, J. B.; Illoh, O.; Kaplan, L. J.; Katz, L. M.; Rao, S. V.; Roback, J. D.; Shander, A.; Tobian, A. A. R.; Weinstein, R.; Swinton McLaughlin, L. G.; Djulbegovic, B. Red Blood Cell Transfusion: A Clinical Practice Guideline From the AABB*. *Ann. Intern. Med.* **2012**, *157*, 49-58.
2. Gray, E. R.; Bain, R.; Varsaneux, O.; Peeling, R. W.; Stevens, M. M., McKendry, R. A.. p24 Revisited: A Landscape Review of Antigen Detection for Early HIV Diagnosis. *AIDS* **2018**, *32*, 2089-2102.
3. Wessman, M. J.; Theilgaard, Z.; Katzenstein, T. L. Determination of HIV Status of Infants Born to HIV-Infected Mothers: A Review of the Diagnostic Methods with Special Focus on the Applicability of p24 Antigen Testing in Developing Countries. *Scand. J. Infect. Dis.* **2012**, *44*, 209-215.
4. Ridzon, R.; Gallagher, K.; Ciesielski, C.; Mast, E. E.; Ginsberg, M. B.; Robertson, B. J.; Luo, C.-C.; DeMaria, A. Simultaneous Transmission of Human Immunodeficiency Virus and Hepatitis C Virus from a Needle-Stick Injury. *N. Engl. J. Med.* **1997**, *336*, 919-922.
5. Kosaka, P. M.; Pini, V.; Ruz, J. J.; da Silva, R. A.; González, M. U.; Ramos, D.; Calleja, M.; Tamayo, J. Detection of Cancer Biomarkers in Serum Using a Hybrid Mechanical and Optoplasmonic Nanosensor. *Nat. Nanotechnol.* **2014**, *9*, 1047.
6. Pini, V.; Kosaka, P. M.; Miguel, F. J. T. D.; Gomez, M. C.; Vega, D. R.; Vidal, O. M.; Martinez, J. J. R.; Pozo, M. E. D. Spectrophotometer. CSIC **2019**, US 10281330 B2.
7. Tamayo de Miguel, F. J., Monteiro-Kosaka, P., Pini, V., Calleja-Gomez, M., Ruz-Martinez, J. J., Ramos-Vega, D., Gonzalez-Sagardoy, M. U. System for biodetection applications. CSIC **2019**, US 10,502,734.

8. Vidarsson, G., Dekkers, G., Rispens, T. IgG Subclasses and Allotypes: From Structure to Effector Functions. *Front. Immunol.* **2014**, *5*, 520.
9. Ruprecht, R. M.; Marasini, B.; Thippeshappa, R. Mucosal Antibodies: Defending Epithelial Barriers against HIV-1 Invasion. *Vaccines* **2019**, *7*, 194.
10. Song, H. Y.; Zhou, X.; Hogley, J.; Su, X. Comparative Study of Random and Oriented Antibody Immobilization as Measured by Dual Polarization Interferometry and Surface Plasmon Resonance Spectroscopy. *Langmuir* **2012**, *28*, 997-1004.
11. Silverton, E. W.; Navia, M. A.; Davies, D. R. Three-Dimensional Structure of an Intact Human Immunoglobulin. *Proc. Natl. Acad. Sci.* **1977**, *74*, 5140-5144.
12. Bertran, O.; Zhang, B.; Schlüter, A. D.; Kröger, M.; Alemán, C. Modeling Nanosized Single Molecule Objects: Dendronized Polymers Adsorbed onto Mica. *J. Phys. Chem. C* **2015**, *119*, 3746-3753.
13. LaGraff, J. R.; Chu-LaGraff, Q. Scanning Force Microscopy and Fluorescence Microscopy of Microcontact Printed Antibodies and Antibody Fragments. *Langmuir* **2006**, *22*, 4685-4693.
14. Zhou, J.; Chen, S.; Jiang, S. Orientation of Adsorbed Antibodies on Charged Surfaces by Computer Simulation Based on a United-Residue Model. *Langmuir* **2003**, *19*, 3472-3478.
15. Liu, J.; Liao, C.; Zhou, J. Multiscale Simulations of Protein G B1 Adsorbed on Charged Self-Assembled Monolayers. *Langmuir* **2013**, *29*, 11366-11374.
16. Cooper, C. D.; Clementi, N. C.; Barba, L. A. Probing Protein Orientation Near Charged Nanosurfaces for Simulation-Assisted Biosensor Design. *J. Chem. Phys.* **2015**, *143*, 124709.

17. R. W. Grawe; Knotts, T. A. The Effects of Tether Placement on Antibody Stability on Surfaces. *J. Chem. Phys.* **2017**, *146*, 215102.
18. Zhou, X.; Wei, S.; Badiyan, S.; Schroeder, M.; Jasensky, J.; Brooks III, C. L.; Marsh, E. N. Investigating the Effect of Two-Point Surface Attachment on Enzyme Stability and Activity. *J. Am. Chem. Soc.* 2018, *140*, 48, 16560–16569.
19. Shen, L.; Schroeder, M.; Ogorzalek, T. L.; Yang, P.; Wu, F.-G.; Marsh, E. N. G.; Chen, Z. Surface Orientation Control of Site-Specifically Immobilized Nitro-reductase (NfsB). *Langmuir* 2014, *30*, 20, 5930–5938.
20. Huff, N. T.; Demiralp, E.; Çagin, T.; Goddard III, W. A. Factors Affecting Molecular Dynamics Simulated Vitreous Silica Structures. *J. Non-Cryst. Solids* **1999**, *253*, 133-142.
21. Todorov, I. T.; Smith, W.; Trachenko, K.; Dove, M. T. DL_POLY_3: New Dimensions in Molecular Dynamics Simulations via Massive Parallelism. *J. Mater. Chem.* **2006**, *16*, 1911-1918.
22. Munetoh, S.; Motooka, T.; Moriguchi, K.; Shintani, A. Interatomic Potential for Si–O Systems Using Tersoff Parameterization. *Comp. Mater. Sci.* **2007**, *39*, 334-339.
23. Sapphire, E. O.; Parren, P. W. H. I.; Pantophlet, R.; Zwick, M. B.; Morris, G. M.; Rudd, P. M.; Dwek, R. A.; Stanfield, R. L.; Burton, D. R.; Wilson, I. A. Crystal Structure of a Neutralizing Human IgG Against HIV-1: A Template for Vaccine Design. *Science* **2001**, *293*, 1155-1159.
24. Case, D. A.; Ben-Shalom, I. Y.; Brozell, S. R.; Cerutti, D. S.; Cheatham-III, T. E.; Cruzeiro, V. W. D.; Darden, T. A.; Duke, R. E.; Ghoreishi, D.; Gilson, M. K.; Gohlke, H.; Goetz, A. W.; Greene, D.; Harris, R.; Homeyer, N.; Huang, Y.; Izadi, S.; Kovalenko, A.; Kurtzman, T.; Lee, T. S.; LeGrand, S.; Li, P.; Lin, C.; Liu, J.; Luchko, T.; Luo, R.;

- Mermelstein, D. J.; Merz, K. M.; Miao, Y.; Monard, G.; Nguyen, C.; Nguyen, H.; Omelyan, I.; Onufriev, A.; Pan, F.; Qi, R.; Roe, D. R.; Roitberg, A.; Sagui, C.; Schott-Verdugo, S.; Shen, J.; Simmerling, C. L.; Smith, J.; Salomon-Ferrer, R.; Swails, J.; Walker, R. C.; Wang, J.; Wei, H.; Wolf, R. M.; Wu, X.; Xiao, L.; York, D. M.; Kollman, P. A. **2018**. AMBER 2018. University of California, San Francisco.
25. Jorgensen, W. L.; Chandrasekhar, J.; Madura, J. D.; Impey, R. W.; Klein, M. L. Comparison of Simple Potential Functions for Simulating Liquid Water. *J. Chem. Phys.* **1983**, *79*, 926-935.
26. Maier, J. A.; Martinez, C.; Kasavajhala, K.; Wickstrom, L.; Hauser, K. E.; Simmerling, C. ff14SB: Improving the Accuracy of Protein Side Chain and Backbone Parameters from ff99SB. *J. Chem. Theory Comput.* **2015**, *11*, 3696-3713.
27. Welch, N. G.; Scoble, J.A.; Muir, B. W.; Pigram, P. J. Orientation and Characterization of Immobilized Antibodies for Improved Immunoassays. *Biointerphases* **2017**, *12*, 02D301.
28. Puiggali-Jou, A.; del Valle, L. J.; Alemán, C.; Pérez-Madrigal, M. M. Weighing Biointeractions between Fibrin(ogen) and Clot-Binding Peptides Using Microcantilever Sensors. *J. Pept. Sci.* **2017**, *23*, 162-171.
29. Lopes-Rodrigues, M.; Puiggali-Jou, A.; Martí-Balleste, D.; del Valle, L. J.; Michaux, C.; Perpète, E. A.; Alemán, C. Thermomechanical Response of a Representative Porin for Biomimetics. *ACS Omega* **2018**, *3*, 7856-7867.
30. Verma, S. K.; Amoah, A.; Schellhaas, U.; Winterhalter, M.; Springer, S.; Kolesnikova, T. A. "To Catch or Not to Catch": Microcapsule-Based Sandwich Assay for Detection of Proteins and Nucleic Acids. *Adv. Funct. Mater.* **2016**, *26*, 6015-6024.

31. Frisch, M. J.; Trucks, G. W.; Schlegel, H. B.; Scuseria, G. E.; Robb, M. A.; Cheeseman, J. R.; Scalmani, G.; Barone, V.; Mennucci, B.; Petersson, G. A.; Nakatsuji, H.; Caricato, M.; Li, X.; Hratchian, H. P.; Izmaylov, A. F.; Bloino, J.; Zheng, G.; Sonnenberg, J. L.; Hada, M.; Ehara, M.; Toyota, K.; Fukuda, R.; Hasegawa, J.; Ishida, M.; Nakajima, T.; Honda, Y.; Kitao, O.; Nakai, H.; Vreven, T.; Montgomery Jr., J. A.; Peralta, J. E.; Ogliaro, F.; Bearpark, M.; Heyd, J. J.; Brothers, E.; Kudin, K. N.; Staroverov, V. N.; Kobayashi, R.; Normand, J.; Raghavachari, K.; Rendell, A.; Burant, J. C.; Iyengar, S. S.; Tomasi, J.; Cossi, M.; Rega, N.; Millam, J. M.; Klene, M.; Knox, J. E.; Cross, J. B.; Bakken, V.; Adamo, C.; Jaramillo, J.; Gomperts, R.; Stratmann, R. E.; Yazyev, O.; Austin, A. J.; Cammi, R.; Pomelli, C.; Ochterski, J. W.; Martin, R. L.; Morokuma, K.; Zakrzewski, V. G.; Voth, G. A.; Salvador, P.; Dannenberg, J. J.; Dapprich, S.; Daniels, A. D.; Farkas, Ö.; Foresman, J. B.; Ortiz, J. V.; Cioslowski, J.; Fox, D. J. **2009**. Gaussian 09, Revision A.1. Gaussian, Inc., Wallingford CT.
32. Yang, L.; Tan, C.-H.; Hsieh, M.-J.; Wang, J.; Duan, Y.; Cieplak, P.; Caldwell, J.; Kollman, P. A.; Luo, R. New-Generation Amber United-Atom Force Field. *J. Phys. Chem. B* **2006**, *110*, 13166-13176.
33. Emami, F. S.; Puddu, V.; Berry, R. J.; Varshney, V.; Patwardhan, S. V.; Perry, C. C.; Heinz, H. Force Field and a Surface Model Database for Silica to Simulate Interfacial Properties in Atomic Resolution. *Chem. Mater.* **2014**, *26*, 2647-2658.
34. Tanner, D. E.; Chan, K.-Y.; Phillips, J. C.; Schulten, K. Parallel Generalized Born Implicit Solvent Calculations with NAMD. *J. Chem. Theory Comput.* **2011**, *7*, 3635-3642.
35. Chwastyk, M.; Cieplak, M. Conformational Biases of alpha-Synuclein and Formation of Transient Knots. *J. Phys. Chem. B* **2020**, *124*, 11-19.

36. Kulke, M.; Uhrhan, M.; Geist, N.; Bruggemann, D.; Ohler, B.; Langel, W.; Koppen, S. Phosphorylation of Fibronectin Influences the Structural Stability of the Predicted Interchain Domain. *J. Chem. Inf. Model.* **2019**, *59*, 4383-4392.
37. Srisvastava, D.; Gakhar, L.; Artemyev, N. O. Structural Underpinnings of Ric8A Function as a G-Protein Alpha-Subunit Chaperone and Guanine-Nucleotide Exchange Factor. *Natur. Commun.* **2019**, *10*, 3084.
38. Mitsutake, A.; Sugita, Y.; Okamoto, Y. Generalized-Ensemble Algorithms for Molecular Simulations of Biopolymers. *Pept. Sci.* **2001**, *60*, 96-123.
39. Sugita, Y.; Okamoto, Y. Replica-Exchange Molecular Dynamics Method for Protein Folding. *Chem. Phys. Lett.* **1999**, *314*, 141-151.
40. Phillips, J. C.; Braun, R.; Wang, W.; Gumbart, J.; Tajkhorshid, E.; Villa, E.; Chipot, C.; Skeel, R. D.; Kalé, L.; Schulten, K. Scalable Molecular Dynamics with NAMD. *J. Comput. Chem.* **2005**, *26*, 1781-1802.
41. Revilla-Lopez, G.; Torras, J.; Nussinov, R.; Aleman, C.; Zanuy, D. Exploring the Energy Landscape of a Molecular Engineered Analog of a Tumor-Homing Peptide. *Phys. Chem. Chem. Phys.* **2011**, *13*, 9986-9994.
42. Mozzi, R. L.; Warren, B. E. The Structure of Vitreous Silica. *J. Appl. Crystallogr.* **1969**, *2*, 164-172.
43. Grimley, D. I.; Wright, A. C.; Sinclair, R. N. Neutron Scattering from Vitreous Silica IV. Time-of-Flight Diffraction. *J. Non-Cryst. Solids* **1990**, *119*, 49-64.
44. Takada, A.; Richet, P.; Catlow, C. R. A.; Price, G. D. Molecular Dynamics Simulations of Vitreous Silica Structures. *J. Non-Cryst. Solids* **2004**, *345-346*, 224-229.

45. Fogarty, J. C.; Aktulga, H. M.; Grama, A. Y.; van Duin, A. C. T.; Pandit, S. A. A Reactive Molecular Dynamics Simulation of the Silica-Water Interface. *J. Chem. Phys.* **2010**, *132*, 174704.
46. D'Souza, A. S.; Pantano, C. G. Mechanisms for Silanol Formation on Amorphous Silica Fracture Surfaces. *J. Am. Ceram. Soc.* **1999**, *82*, 1289-1293.
47. Wang, H.; Castner, D. G.; Ratner, B. D.; Jiang, S. Probing the Orientation of Surface-Immobilized Immunoglobulin G by Time-of-Flight Secondary Ion Mass Spectrometry. *Langmuir* **2004**, *20*, 1877-1887.
48. Tajima, N.; Takai, M.; Ishihara, K. Significance of Antibody Orientation Unraveled: Well-Oriented Antibodies Recorded High Binding Affinity. *Anal. Chem.* **2011**, *83*, 1969-1976.

TOC

